Journal of Solid State Chemistry 182 (2009) 3393–3398

Contents lists available at ScienceDirect

Journal of Solid State Chemistry

journal homepage: www.elsevier.com/locate/jssc

Enhancement mechanism of field electron emission properties in hybrid carbon nanotubes with tree- and wing-like features

G.M. Yang [a,b], C.C. Yang [b,*], Q. Xu [c], W.T. Zheng [a,*], S. Li [b]

[a] Department of Materials Science, State Key Laboratory of Superhard Materials, and Key Laboratory of Automobile Materials of MOE, Jilin University, Changchun 130012, PR China
[b] School of Materials Science and Engineering, The University of New South Wales, NSW 2052, Australia
[c] Changchun Institute of Technology, Changchun 130021, PR China

ARTICLE INFO

Article history:
Received 17 June 2009
Received in revised form
4 October 2009
Accepted 11 October 2009
Available online 17 October 2009

Keywords:
Branch
Density
Graphitic sheets
RF-PECVD

ABSTRACT

In this work, the tree-like carbon nanotubes (CNTs) with branches of different diameters and the wing-like CNTs with graphitic-sheets of different densities were synthesized by using plasma enhanced chemical vapor deposition. The nanostructures of the as-prepared hybrid carbon materials were characterized by scanning electron microscopy and transmission electron microscopy. The structural dependence of field electron emission (FEE) property was also investigated. It is found that both of the tree- and wing-like CNTs exhibit a lower turn-on field and higher emission current density than the pristine CNTs, which can be ascribed to the effects of branch size, crystal orientation, and graphitic-sheet density.

1. Introduction

In the past two decades, carbon nanotubes (CNTs) as one of the most promising candidates in field emission devices have drawn great attentions due to their unique physicochemical properties, small curvature radius, high thermal stability, high electrical conductivity, etc. [1–3]. To develop CNT-based field emission devices, low turn on field, high current densities, and the uniformity over a large area need to be achieved. For this purpose, a number of experimental efforts have been implemented to synthesize the hybrid CNTs with the enhancing field electron emission (FEE) properties [4–8]. For example, arc discharge [5], plasma enhanced chemical vapor deposition (PECVD) and thermal CVD [2], nano-agglomerate fluidized bed reactor and floating catalytically CVD (NAFBR-FCCVD) [6], and direct current (dc)-CVD [7] have been widely used for the preparation of tree-like CNT composites with CNT branches on the surface of the pristine CNTs. However, most of these efforts are facing two challenging issues, i.e., a low formation efficiency of hybrid structures and uncontrollable synthesis process, which may be due to that (1) the aggregation of pre-loaded nanosized particles is difficult to be eliminated completely, thus restraining the growth of the branches on the CNTs; and (2) the prepared CNTs randomly distribute in the tree-like CNT composite, which depresses their FEE properties. One way to solve these problems is to grow the thick CNTs as supports [8,9]. The other way is to prepare the wing-like CNTs [10,11]. However, up to date, the FEE properties of the wing-like CNTs have not been investigated, and the mechanism underlying the enhancement of FEE properties in the tree- and wing-like CNTs is unclear. This has impeded the rapid development of CNT-based field-emission devices.

In this work, both the tree- and wing-like CNTs were synthesized using radio frequency (RF)-PECVD, where (1) the branch diameters of the tree-like CNTs are controlled by changing the quantity of ferrocene contents; and (2) the graphitic sheet density of the wing-like CNTs is controlled by the deposition time. The effects of the branch diameter, crystal orientation, and graphitic sheet density on the FEE properties of the synthesized CNTs were studied. The growth mechanism of the wing-like CNTs is also investigated.

2. Experimental section

The tree-like CNTs are defined as thin CNTs grown on the trunk or tips of pristine CNTs, whereas the graphitic sheets on CNTs are named as wing-like CNTs in this work. The tree-like CNTs were prepared by the RF-PECVD and Fig. 1 shows a schematic illustration of the RF-PECVD apparatus used in our experiments (RF power: 13.56 MHz) and the vapor-phase transport process of Fe nanoparticles decorated on vertically aligned CNTs. To

* Corresponding authors. Fax: +61 2 93855956 (C.C. Yang); +86 431 85168246 (W.T. Zheng).
E-mail addresses: ccyang@unsw.edu.au (C.C. Yang), wtzheng@jlu.edu.cn (W.T. Zheng).

0022-4596/$ - see front matter © 2009 Elsevier Inc. All rights reserved.
doi:10.1016/j.jssc.2009.10.005

synthesize the tree-like CNTs with different branch diameters, high-purity ferrocene powders (0.005, 0.01, and 0.02 g, respectively) were put into a ceramic tube with a diameter of 6 mm through a small hole at the center of one end of the tube. The hole was then covered by a piece of Al plate tightened with Al wires to avoid rapid decomposition of the ferrocene. The as-prepared pure CNTs on Si (1 0 0) substrates were placed in the downstream site along the vapor flow direction at a distance of 4 mm from the ceramic tube. During the deposition, a radio frequency power of 230 W was utilized and the substrate temperature was kept at 800 °C. The flow rate ratio of CH_4 and H_2 gas is 80/20 sccm. After 20-min deposition, CH_4 inlet was shutoff and the system was cooled down to room temperature.

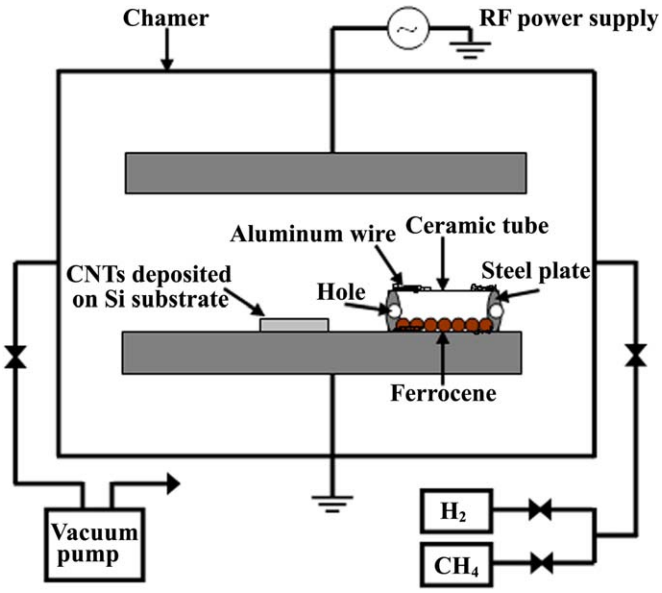

Fig. 1. Vapor-phase transport process for Fe nanoparticles decorated on vertically aligned pristine CNTs.

To grow the wing-like CNTs, Ti thin film with a thickness of ~20 nm was deposited on Si (100) substrate using magnetron sputtering, and then the Co thin film with a thickness of ~15 nm as a catalyst was coated on the surface of Ti thin film. In order to compare the catalyst activity, the Ni as catalyst is also used to grow CNTs. The RF-PECVD chamber was evacuated to a pressure of 8.0 Pa, and then pure hydrogen (99.99%) at the flow rate of 20 sccm was then introduced into the chamber. After the Si substrate was heated to 800 °C for 40 min, pure CH_4 (99.99%) with a gas flow rate of 80 sccm was purged into the chamber. A working pressure of 800 Pa and a radio frequency power of 230 W were utilized to grow the wing-like CNTs with the deposition time of 10, 15, and 30 min, respectively. After the deposition, the CH_4 inlet was shutoff and the system was cooled to room temperature in a H_2 atmosphere.

The as-prepared materials were characterized by scanning electron microscopy (SEM) (JEOL JSM-6700F), Raman spectroscopy (Renishaw-inVia with 514 nm excitation wavelength), transmission electron microscope (TEM) (Hitachi H-8100), and high resolution transmission electron microscope (HRTEM) (JEOL TEM-2010). The TEM and HRTEM samples were prepared by scratching the surface of the as-prepared sample using a sharp tungsten tip and depositing the collected material on a copper TEM grid. The FEE properties were measured using a parallel plate configuration, an indium-tin-oxide (ITO) anode and a cathode (the sample) in a vacuum chamber maintained at a pressure of 1.2×10^{-7} Pa.

3. Results and discussion

Figs. 2(a–c) show the SEM images of tree-like CNTs with branches having different diameters, from which the diameters and lengths of pristine CNTs are about 15–70 nm and 2 μm,

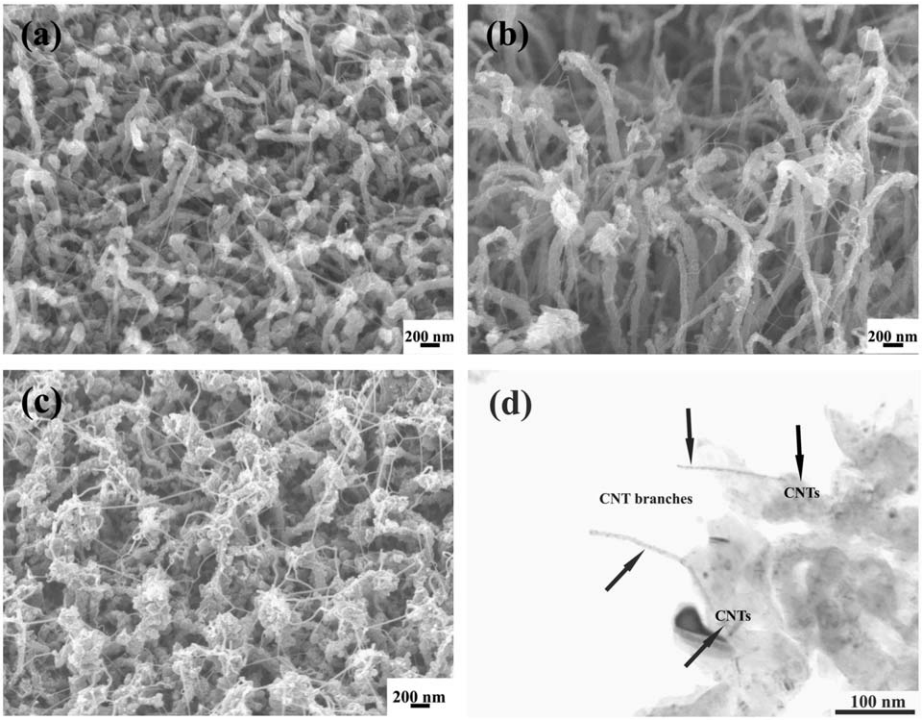

Fig. 2. SEM images of tree-like CNTs with branches having different diameters: (a) 4, (b) 6, and (c) 20 nm, respectively, and (d) the corresponding TEM image of branch and CNT denoted by arrows in (b).

respectively. After the CNTs are decorated with catalyst (Fe nanoparticles), the nucleation and growth of thin CNTs around the particles take place. The branches of CNTs are on the surfaces or the tips of as-prepared CNTs, whose diameters are about 4, 6, and 20 nm (Figs. 2(a, b, c), respectively), respectively. Fig. 2(d) is a typical TEM image of the tree-like CNTs with branches having a diameter of 6 nm. From SEM images, the branch diameters of CNTs increase with increasing ferrocene content. In this work, when the CH_4 content reaches to a critical point, carbon atoms quickly become saturated for the Fe nanoparticles due to the solubility limit of carbon in Fe and the segregation of carbon atoms occurs, which determines the type of final composite products. In the process of the segregation of carbon atoms, the CNTs grow continuously [12,13]. It has been found that the hydrogen atmosphere, carbon source, and catalyst play important roles in the growth of tree-like CNTs [14]. In this work, although the flow rate ratio of H_2/CH_4 is high, which leads to that ionized H_2 etches the CNT branches severely due to the hydrogen plasma irradiation, CNT branches still grow from the surface of CNT trunks. This may be associated with that small catalyst Fe particles are active.

Fig. 3 exhibits the normalized Raman spectra for pristine CNTs and tree-like CNTs in the range of 0–2000 cm^{-1}. Two characteristic bands can be found in each spectrum, i.e., disorder graphitic D-band at 1350 cm^{-1}, and G-band related to in-plane sp^2 vibrations at 1580 cm^{-1} [11,15,16]. The disorder D-band in CNTs is primarily caused by the defects in the tube wall, such as bending in the CNTs, the finite size of crystalline domains, sp^3-hybridized bonds, and functional groups created by the oxidation [17–19]. The intensity ratio of D- over G-band, $R=I_D/I_G$, is estimated, which characters the degree of disorder in the structures of carbonaceous materials. The R values for the pristine CNTs, and the tree-like CNTs with a branch diameter of 4, 6, and 20 nm, respectively, are 0.65, 0.72, 0.81, and 0.96, respectively. It is evident that the degree of disorder in the walls of CNTs substantially increases with an increase in the branch diameters or ferrocene content. All tree-like CNTs have higher disorder than the pristine CNTs, which is attributed to the Fe nanoparticles coated on the walls of CNTs in the vapor phase transport process. The Fe atoms have a coordinative affinity to the surface of CNTs and dissolve the walls of CNTs at high temperature. In addition, the walls of CNTs are oxidated by oxygen atoms or clusters from ferrocene decomposition. As a result, the surface of CNTs is oxidated more severely with an increase in ferrocene content. Moreover, the C–H bonds on the walls of CNTs could be deformed by the hydrogen atoms existing in the chamber at a temperature of 800 °C and the hydrogen plasma etching on the pristine CNTs during the pyrolysis of ferrocene. This causes a hybridized carbon transfer from sp^2 to sp^3 on the walls of CNTs during the deposition process. Such a phenomenon also contributes to the higher R values of tree-like CNTs.

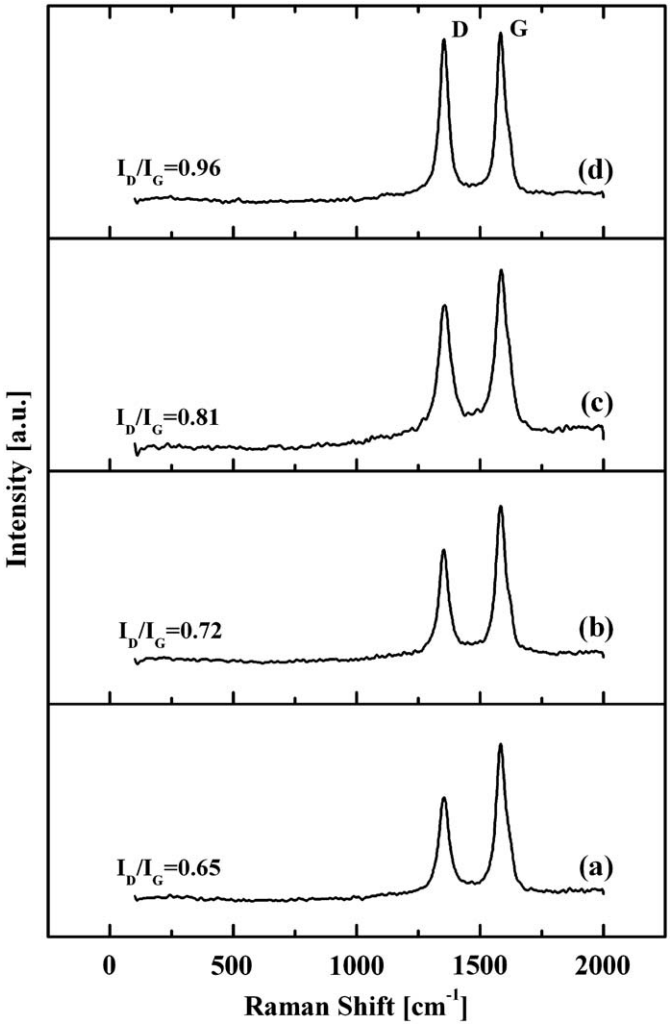

Fig. 3. Raman spectra of (a) pristine CNTs (Curve A) and tree-like CNTs with branches having different diameters: (b) 4, (c) 6, and (d) 20 nm, respectively (Curves B, C, and D).

Figs. 4(a–c) show the SEM images of the Co-catalyzed wing-like CNTs with graphitic sheets having different densities grown at 800 °C for 10, 15, and 30 min, respectively, in which the insets in Figs. 4(a) and (c) show the lengths of the corresponding CNTs. The diameter and length of the CNTs are about 30 nm and 2 μm, respectively. With increasing deposition time, the density of the graphitic sheets on CNTs increases, while the average length of the CNTs is almost time-independent. No nanosheets grow on the CNTs using Ni as a catalyst in this work although the synthesis conditions are the same as those for depositing wing-like CNTs for 30 min using Co as a catalyst, which is a consequence of that the catalyst Ni is more active than Co. Thus the catalysts may play an important role in the growth of graphitic nanosheets.

Fig. 5 exhibits the normalized Raman spectra for wing-like CNTs using Co as a catalyst grown for (a) 10, (b) 15, and (c) 30 min, respectively. Two characteristic bands, D and G, can also be observed in each spectrum, which is similar to those for tree-like CNTs. The R values for the wing-like CNTs grown for 10, 15, and 30 mins, respectively, are 0.59, 0.82, and 0.97, respectively, showing a substantial increase in the degree of disordering in the walls of CNTs as deposition time increases. This may be caused by the partial transfer of hybridized carbon from sp^2 to sp^3 on the walls of CNTs during deposition. The difference in R-value between the wing-like CNTs grown for 15 and 30 min is much smaller than that between for 10 and 15 min, although the time interval is longer for the former. This implies that the formation of nanosheets on the walls of CNTs can protect CNT walls from a further damage.

Figs. 6(a) and (b) are the TEM images for the wing-like CNTs grown for 15 and 30 min, respectively, where well-dispersed graphitic sheets grow on the sidewalls of CNTs. The nanosheets emanate from the cylindrical surface of the CNTs and protrude up to about 20 nm from the CNT surface at an angle of 20–120° along with the tube axis. Moreover, Fig. 6(b) evidences the hollow structure of the as-prepared CNTs. Figs. 6(c) and (d) show the TEM images for the nanosheets denoted by arrows in Fig. 6(b), from which the nanosheets are roughly ordered and seem to connect continuously with the walls of the CNTs.

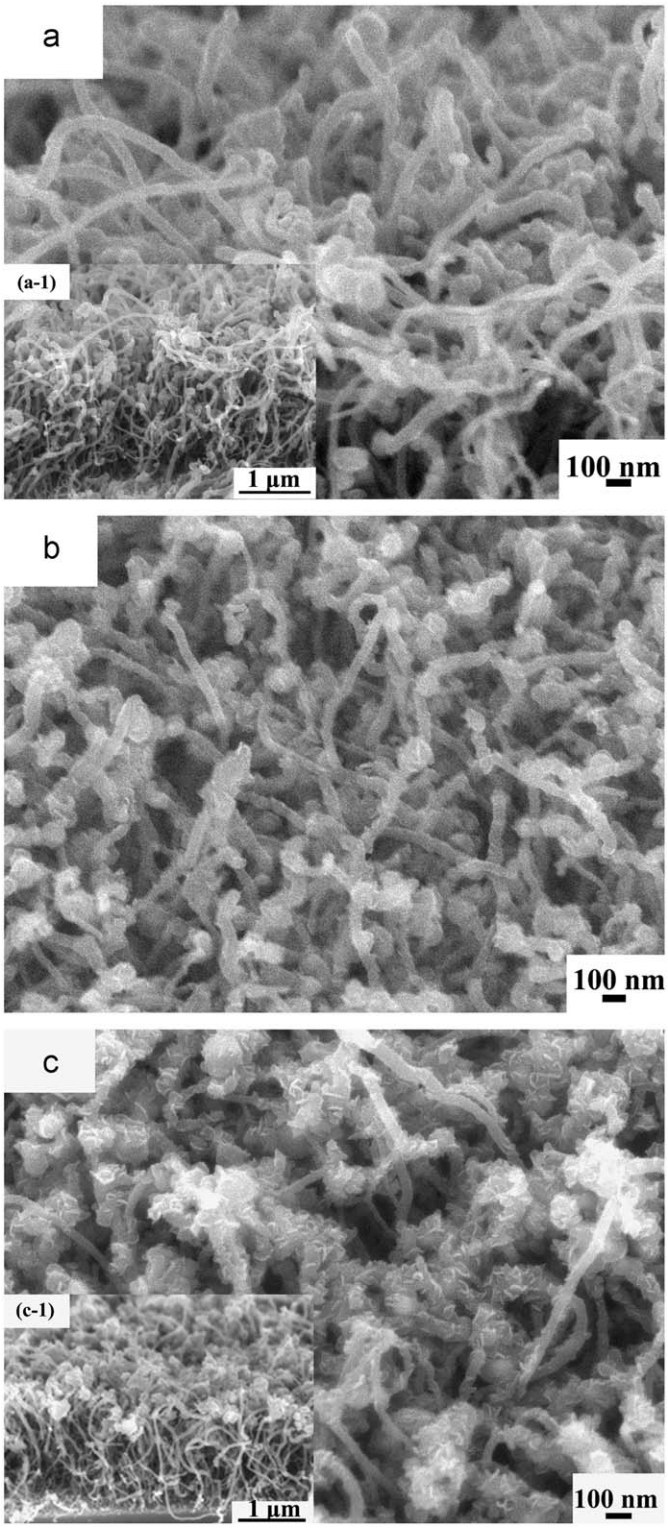

Fig. 4. SEM images of Co-catalyzed wing-like CNTs tilted at 45° grown for (a) 10, (b) 15, and (c) 30 min, respectively, from which the insets (a-1) and (c-1) exhibit the corresponding SEM images of (a) and (c), tilted at 70°.

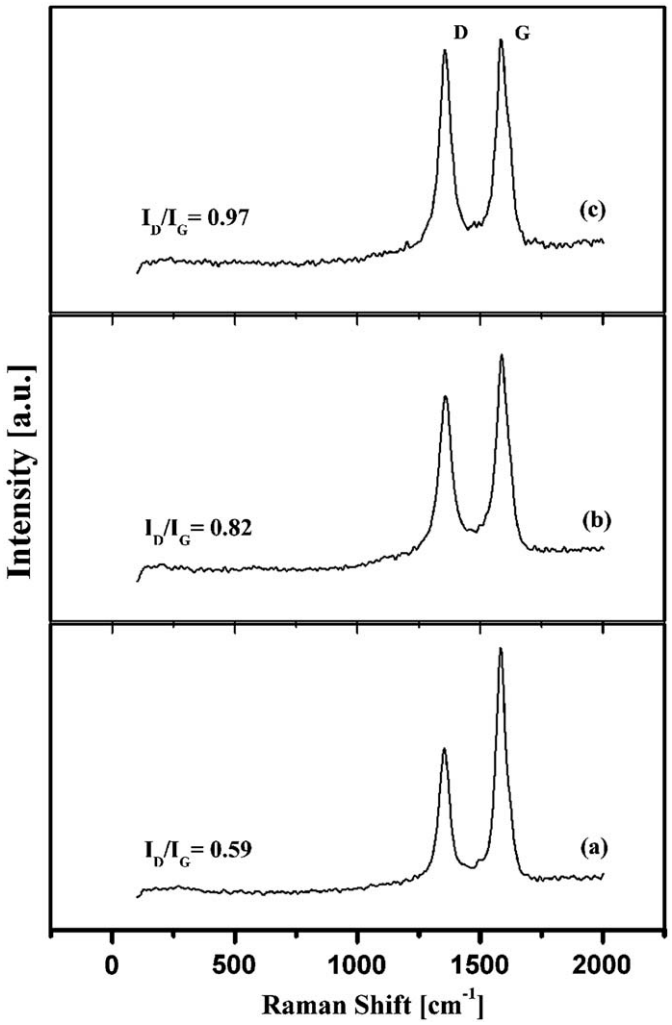

Fig. 5. Raman spectra of wing-like CNTs grown for (a) 10, (b) 15, and (c) 30 min, respectively.

A competitive growth mechanism between CNTs and graphite sheets is proposed as follows: at the initial stage of deposition, CNTs grow very fast due to the high activity of catalyst Co. With increasing deposition time, the activity of catalyst Co is lowered and the abundant carbon radicals rapidly accumulate, thus impeding the further growth of CNTs. In this case, the carbon radicals inserted into the side walls/tips of the tubes form more and more graphite sheets, as shown in Figs. 4(b) and (c). On the other hand, the high temperature is also one of the important factors for forming graphitic nanosheets since carbon nanomaterials prefer to form amorphous structure at low temperature [10]. Moreover, the hydrogen in the plasma is also critical for forming nanosheets. In addition, during the growth of CVD nanotubes, structural defects and non-hexagonal member rings (topological lattice defects) are always observed. These defects are highly reactive and sensitive to the plasma etching, and therefore may provide nucleation sites for nanosheets [20,21]. It seems that there are two competitive effects to influence the nanosheets growth. One is the deposition of the carbon-based ions, and another is the etching effect caused by the hydrogen ions. With low hydrogen content in the discharge gases, the deposition rate of carbon-based ions is higher than the etching rate, resulting in that the graphite sheets form.

Fig. 7(a) plots the FEE current density as a function of electric field for pure CNTs (A) and the tree-like CNTs with branches having a diameter of 4 (B), 6 (C), and 20 nm (D), respectively, as well as the wing-like CNTs grown for 10 (E), 15 (F), and 30 min (G), respectively. The turn-on electric fields, which are corresponding to an electron emission density of 10 μA/cm^2, can be determined

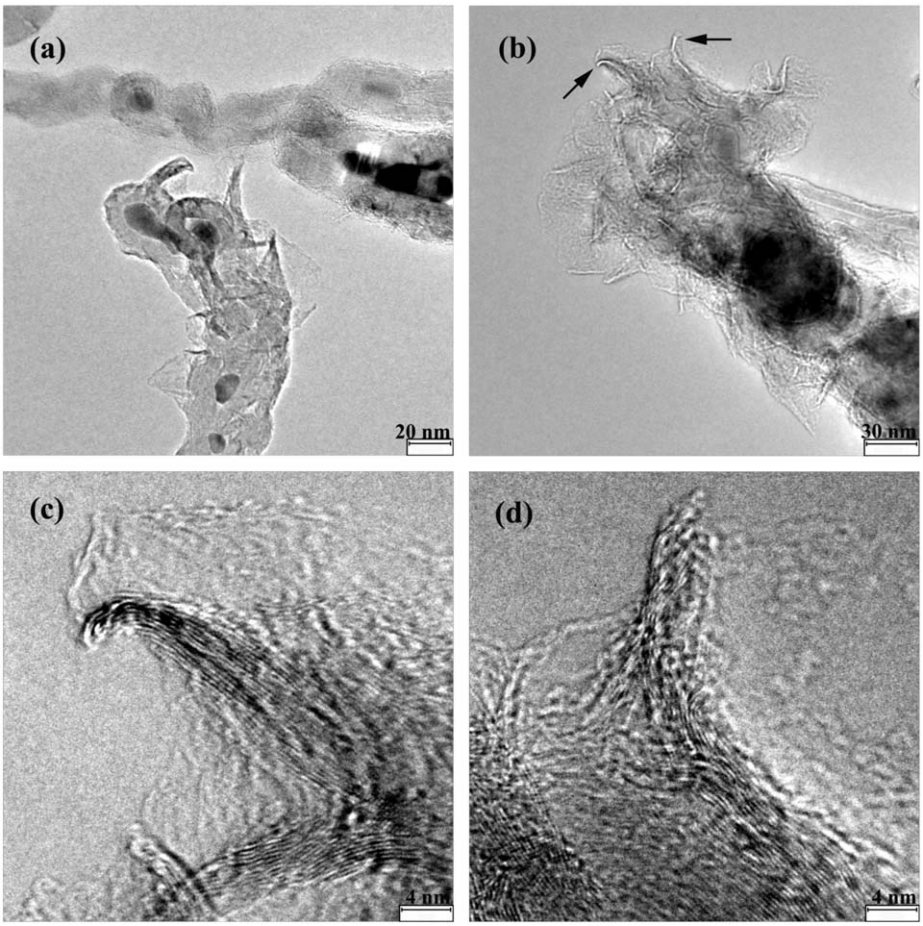

Fig. 6. TEM images of wing-like CNTs grown for (a) 15 and (b) 30 min, respectively, and (c) and (d) are the corresponding TEM images of nanosheets denoted by arrows in (b).

in Fig. 7(a). The results and the characteristic parameters associated with the FEE property of CNTs are listed in Table 1. From this table, the turn-on fields for samples B, C, and D are all much lower than that for sample A, indicating that the tree-like CNTs have much better FEE properties compared to pure CNTs. This is attributed to the tip effect in the tree-like CNTs. It is reported that the amplification factor of the tip is approximately 125 times as large as that of the nanotube body [22]. As shown in Fig. 2(d), the branches appear on the as-prepared CNTs for our obtained samples, acting as the tips. These branches provide more electrons emission sites to enhance the FEE properties of tree-like CNTs than pure CNTs. In general, the emission current density is inversely proportional to the square of the emitter radius [3]. In this work, the FEE property of sample B should be better than that of C due to that sample B has a smaller branch diameter. However, the turn-on field of the sample C is lower than that of either sample B or D. Also, sample C has the highest emission current density among seven samples. This can be explained by the well oriented branches in sample C. From Table 1, it is worth noting that sample B has a better FEE property than sample D, which can be attributed to that sample B has much smaller branch (4 nm) than D (20 nm).

From Fig. 7(a) and Table 1, the wing-like CNTs grown for 15 min (sample F) have the highest emission current density among samples E, F, and G. Compared with sample E, the graphite sheets in sample F are well mixed with CNTs, resulting in the formation of more tips on the sidewall or tips of CNTs. This leads to that sample F has better FEE properties than sample E. However, as deposition time increases up to 30 min, too many nanosheets almost cover the tips of CNTs, impeding the FEE. Consequently, sample F has better FEE properties than sample G. Furthermore, too many nanosheets produced by relatively long deposition time (e.g., 30 min) shield all surfaces of CNTs, causing an increase in the diameters of CNTs [3] and a decrease in the tip emission of the CNTs, as well as an increase in the electrostatic screen effect [23]. This result in a depressed emission performance compared to pure CNTs.

As shown in Fig. 7(b), the Fowler–Nordheim (F–N) plots of samples A–G observe the Fowler–Nordheim equation as follows: $\ln(J/E^2) = \ln(A\beta^2/\varphi) - B\varphi^{3/2}/\beta E$, where $A = 1.54 \times 10^{-6}\,\mathrm{A\,eV\,V^{-2}}$ and $B = 6.83 \times 10^3\,\mathrm{eV^{-3/2}\,V\,\mu m^{-1}}$, $\beta = -B\varphi^{3/2}/S_{FN}$ is the field enhancement factor with S_{FN} being the slope of the FN plots, and φ is the work function of emitters. With $\varphi_{CNT} = 5.0$ eV, the β values are estimated and listed in Table 1, from which the β value of the pristine CNTs is much smaller than that of either tree- or wing-like CNTs except for sample G. The reason is that most of the tips on CNTs for sample G are covered by too many nanosheets, as noted before.

4. Conclusions

A simple technique has been developed to synthesize the tree- and wing-like hybrid CNTs using PECVD. The FEE properties for these hybrid materials have been significantly enhanced compared with pristine CNTs. The diameters of the branches and

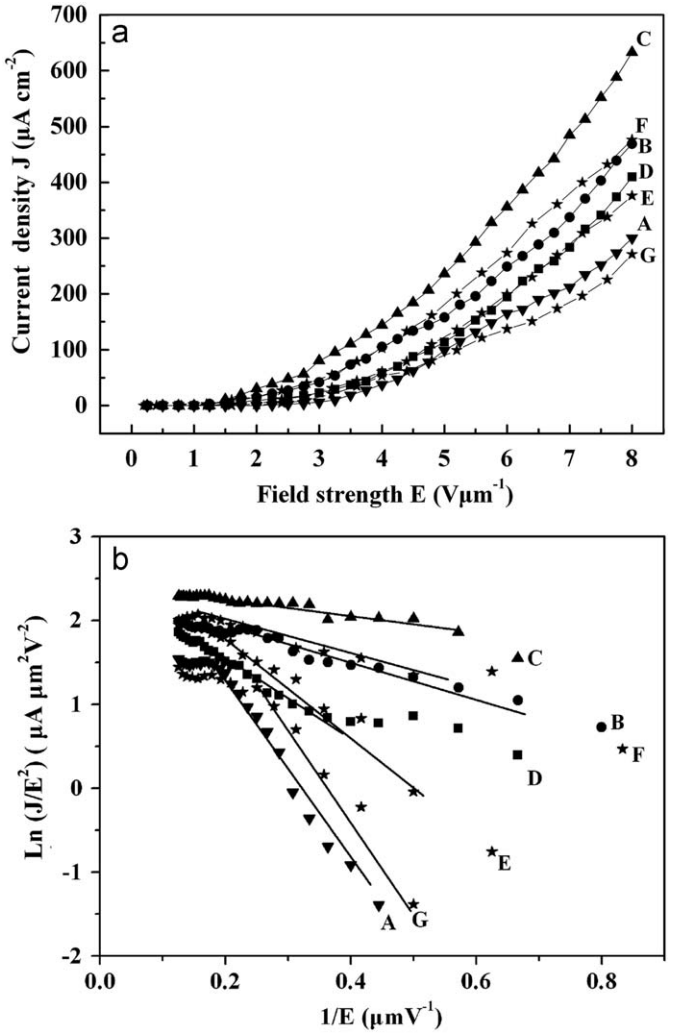

Fig. 7. (a) Field emission current density as a function of electric field for (A) pure CNTs, tree-like CNTs with branches having different diameters: (B) 4, (C) 6, and (D) 20 nm, respectively, as well as wing-like CNTs grown for (E) 10, (F) 15, and (G) 30 min, respectively, and (b) Fowler–Nordheim (F–N) plots corresponding to samples A–G.

branch alignment in CNTs are the main factors to influence the FEE properties of tree-like CNTs. In contrast, the graphitic-sheet density in CNTs may play a key role in determining the FEE properties of wing-like CNTs. The findings in this work provide a design principle for developing CNT-based nanomaterials with superior field electron emission properties and new insight into their potential applications as field emission devices.

Table 1
Characteristic parameters of samples A–G associated with their FEE properties.

Sample	D or T	Alignment	R	V (V μm^{-1})	J (μA cm^{-2})	β
A	/	/	0.65	3	300	7.5×10^3
B	4 nm	Not good	0.72	1.7	470	3.1×10^4
C	6 nm	Good	0.81	1.3	633	4.2×10^4
D	20 nm	Not good	0.96	2.1	410	1.6×10^4
E	10 min	/	0.59	2.3	376	1.4×10^4
F	15 min	/	0.82	1.6	477	3.9×10^4
G	30 min	/	0.97	2.9	271	7×10^3

D denotes the branch diameter, T deposition time, R crystallinity, V turn on field, J current density at 8 V μm^{-1}, and β field enhancement factor.

Acknowledgments

The authors would like to thank the supports from National Natural Science Foundation of China (Grant nos. 50832001 and 50525204), and special Ph.D. program from Chinese Education Ministry (Grant no. 200801830025).

References

[1] S. Iijima, Nature 354 (1991) 56.
[2] H.J. Kim, I.T. Han, P.Y. Jun, J.M. Kim, J.B. Park, B.K. Kim, N.S. Lee, Chem. Phys. Lett. 396 (2004) 6.
[3] H.Y. Jung, S.M. Jung, L. Kim, J.S. Suh, Carbon 46 (2008) 969.
[4] L.P. Biro, Z.E. Horvath, G.I. Mark, Z. Osvath, A.A. Koos, A.M. Benito, W. Maser, P. Lambin, Diamond Relat. Mater. 13 (2004) 241.
[5] D. Zhou, S. Seraphin, Chem. Phys. Lett. 238 (1995) 286.
[6] H. Yu, Z. Li, G. Luo, F. Wei, Diamond Relat. Mater. 15 (2006) 1447.
[7] Y. Abdi, S. Mohajerzadeh, J. Koohshorkhi, M.D. Robertson, C.M. Andrei, Carbon 46 (2008) 1611.
[8] X. Sun, R. Li, B. Stansfield, J.P. Dodelet, S. Desilets, Chem. Phys. Lett. 394 (2004) 266.
[9] G.M. Yang, X. Wang, Q. Xu, S.M. Wang, H.W. Tian, W.T. Zheng, J. Solid State Chem. 182 (2009) 966.
[10] S. Trasobares, C.P. Ewels, J. Birrell, O. Stephan, B.Q. Wei, J.A. Carlisle, D. Miller, P. Keblinski, P.M. Ajayan, Adv. Mater. 16 (2004) 610.
[11] A. Malesevic, S. Vizireanu, R. Kemps, A. Vanhulsel, C.V. Haesendonck, G. Dinescu, Carbon 45 (2007) 2932.
[12] W.Z. Li, S.S. Xie, L.X. Qian, B.H. Chang, B.S. Zou, W.Y. Zhou, Science 274 (1996) 1701.
[13] M. Meyyappan, L. Delzeit, A. Cassell, D. Hash, Plasma Sources Sci. Technol. 12 (2003) 205.
[14] J.W. Liu, X. Wang, W.T. Zheng, J.X. Li, Q.F. Guan, Y.D. Su, J.L. Qi, Q. Jiang, Carbon 45 (2007) 668.
[15] E.T. Thostenson, W.Z. Li, D.Z. Wang, Z.F. Ren, T.W. Chou, J. Appl. Phys. 91 (2002) 6034.
[16] Q.T. Li, Z.C. Ni, J.L. Gong, D.Z. Zhu, Z.Y. Zhu, Carbon 46 (2008) 434.
[17] W.Z. Li, H. Zhang, C.Y. Wang, Y. Zhang, L.W. Xu, K. Zhu, S.S. Xie, Appl. Phys. Lett. 70 (1997) 2684.
[18] A. Hirsch, Angew. Chem. Int. Ed. 41 (2002) 1853.
[19] A.C. Ferrari, J. Robertson, Phys. Rev. B 61 (2000) 14095.
[20] A.V. Krasheninnikov, K. Nordlund, M. SirviO, E. Salonen, J. Keinonen, Phys. Rev. B 63 (2001) 245405.
[21] J.A.V. Pomoell, A.V. Krasheninnikov, K. Nordlund, J. Keinonen, J. Appl. Phys. 96 (2004) 2864.
[22] G. Zhou, W. Duan, B. Gu, Appl. Phys. Lett. 79 (2001) 836.
[23] L. Nilsson, O. Groening, C. Emmenegger, O. Kuettel, E. Schaller, L. Schlapbach, H. Kind, J.-M. Bonard, K. Kern, Appl. Phys. Lett. 76 (2000) 2071.